Doctor of Philosophy

Analysis of Left Ventricular Mass and Position of Papillary Muscle in Patients with Hypertrophic Cardiomyopathy, Using Three-Dimensional Reconstruction of Cardiac Computed Tomography

The Graduate School

of the University of Ulsan

Department of Medicine

Choi, Suk-Won

Analysis of Left Ventricular Mass and Position of Papillary Muscle in Patients with Hypertrophic Cardiomyopathy, Using Three-Dimensional Reconstruction of Cardiac Computed Tomography

Supervisor: Song, Jae-Kwan

A Dissertation

Submitted to

the Graduate School of the University of Ulsan

in Partial Fulfillment of the Requirements

for the Degree of

Doctor of Philosophy

by

Choi, Suk-Won

Department of Medicine

Ulsan, Korea

August 2019

Analysis of Left Ventricular Mass and Position of Papillary Muscle in Patients with Hypertrophic Cardiomyopathy, Using Three-Dimensional Reconstruction of Cardiac Computed Tomography

This certifies that the dissertation

of Suk-Won Choi is approved.

Yang, Dong-Hyun
Committee Chair Dr.

Song, Jae-Kwan
Committee Member Dr.

Song, Jong-Min
Committee Member Dr.

Jung, Sung-Ho
Committee Member Dr.

Ryu, Kyu-Hyung
Committee Member Dr.

Department of Medicine
Ulsan, Korea
August 2019

Abstract

Background: Hypertrophic cardiomyopathy is an inherited disorder characterized by increased myocardial mass, of which pathologic hallmark is left ventricular outflow tract (LVOT) obstruction. We aimed to evaluate the contribution of in-vivo left ventricle (LV) and papillary muscle (PM) mass and the displacement of both PMs to LVOT obstruction by using reconstructed three-dimensional (3D) cardiac computed tomography (CT) images.

Methods and Results: A total of 90 patients with HCM – 30 patients with asymmetric septal hypertrophy (ASH) with LVOT obstruction, 30 patients with ASH only, and 30 patients with apical HCM - and 30 normal controls, who performed cardiac CT and two-dimensional echocardiography, were retrospectively enrolled. Using customized software (A-View, Cardiac, Asan Medical Center, Korea), we obtained cardiac CT images and drew LV masks by using the difference of Hounsfield unit and corrected LV masks manually according to LV myocardium. After completing the masks of the LV and the PMs, we calculated LV and PM mass. We realigned XYZ-coordinates of the LV by positioning LV apex to inferior and LV base to superior. We calculated 3D coordinates of the tip and the barycenter of both PMs and analyzed the displacement of each point among study groups. Mass of both PMs, indexed to body surface area, was significantly increased in the order named; the group of normal control, apical HCM, ASH only, and ASH with LVOT obstruction. The pattern of hypertrophy of both PM seemed to be different that the anterolateral PM gets elongated, while the posteromedial PM gets thicker. The ratio of anterolateral PM mass to posteromedial PM mass and the

difference of both PM mass seemed to increase sequentially as LV mass increases. The only independent predictor of LVOT obstruction was from medial to lateral displacement of the barycenter of the posteromedial PM. (adjusted odds ratio 0.808, 95% confidence interval 0.718-0.909, *P* value <0.001)

Conclusions: From complete 3D masks of the LV and the PMs from cardiac CT images, we could identify that the mass of both PMs increases and the ratio of mass of the anterolateral PM to that of the posteromedial PM also increases as LV mass increases. The only independent predictor of LVOT obstruction was from medial to lateral displacement of the barycenter of the posteromedial PM, which might result from the pattern of hypertrophy of the posteromedial PM.

Contents

Lists of tables

Lists of figures

INTRODUCTION

Hypertrophic cardiomyopathy (HCM) is a inherited disorder characterized by increased myocardial mass.[1] It is caused by mutations of sarcometric genes with anatomical, hemodynamic and clinical phenotypes, including asymmetric septal hypertrophy (ASH), midventricular hypertrophy, and apical hypertrophy.[2,3] Recently, it has been recognized that HCM is not characterized solely by ventricular hypertrophy, but a number of abnormalities of the mitral apparatus. Although its clinical presentation ranges from asymptomatic status to progressive heart failure or sudden death,[4,5] pathological hallmark of HCM is left ventricular outflow tract (LVOT) obstruction due to structural and functional abnormalities of the mitral apparatus. Previously, several distinguishing features associated with LVOT obstruction have been investigated such as mitral valve (MV) systolic anterior motion (SAM),[6,7] LVOT narrowing,[8] hyperdynamic ejection,[9] and increased mitral leaflet area.[10-12] Among them, a number of papillary muscle (PM) abnormalities - in particular PM hypertrophy,[13] anterior and medial displacement of both PMs,[14-18] accessory PMs,[13] doubly bifurcated PMs[19,20] - have been highlighted.

A recent study, using 3-dimensional (3D) echocardiography, revealed geometric determinant of LVOT obstruction that included mitral leaflet area and papillary muscle displacement.[17] In the context of papillary muscle displacement, medial displacement toward the center of the mitral annulus and anterior displacement of both PMs was revealed to be a independent determinant of LVOT obstruction in patients with ASH and LVOT obstruction. However, although 3D echocardiography has an advantage of assessing the MV apparatus owing to high temporal resolution, it is somewhat limited in evaluating entire left ventircular myocardium and the PMs. In addition, this study used tips of both PMs as an indicator of PM displacement. Obviously, the tips of both PMs do not seem to embody whole PMs and a further study, using other points which can represent positions of the PMs in the left ventricle (LV), are required to understand the mechanism between LVOT obstruction and PM geometry.

Cardiac computed tomography (CT) has greatly advanced as an accurate and reliable tool for assessing global LV function beyond coronary arteries.[21] Further more, because of its high spatial resolution, anatomic details of the MV and subvalvular apparatus can be visualized.[22] In a previous study which used cardiac CT, LVOT obstruction was independently associated with a spiral pattern of LV hypertrophy, a longer anterior mitral leaflet length, and a longer distance from lateral PM base to LV apex.[23] Counterclockwise spiral rotation of hypertrophy was significantly common in patients with HCM and LVOT obstruction when viewed from the LV apex along the basal to apical direction. Also, by demonstrating that a longer distance from lateral PM base to LV apex was a significant predictor of LVOT obstruction, the authors suggested that displacement of anterolateral PM might be important in the pathophysiology of LVOT obstruction. However, they measured the distance between PM base and LV apex in the two-dimensional images of cardiac CT, which might be different from real distance in the 3D model, and the base of both PMs are ambiguous to locate the exact point due to their intrisic morphology which separates into several branches on the ventricular endocardium.

In this study, using cardiac CT images, we reconstructed complete 3D LV myocardium including both PMs with customized software (A-View Cardiac, Asan Medical Center, Korea). With the 3D reconstructed images, we aimed to evaluate the contribution of in-vivo LV/ PM mass and the displacement of both PMs to LVOT obstruction by calculating 3D-coordinates of tips and centers of mass of the PMs. We chose and calculated the center of mass (barycenter) as an alternative to tip and base of the PM for representing the position of whole PM. The center of mass is a useful reference point for calculations in mechanics that involve masses distributed in space.

METHODS

Study population

Between June 2011 and May 2016, a total of 90 patients with HCM (myocardial thickness ≥ 15 mm on two-dimensional [2D] echocardiography) and 30 normal controls, who performed cardiac CT and 2D echocardiography, were retrospectively enrolled. Among patients with HCM, 30 patients had asymmetric septal hypertrophy (ASH) with LVOT obstruction on 2D echocardiography, 30 patients with ASH only, and 30 patients with apical HCM. The institutional review board approved this retrospective study and waived the requirement to obtain informed consent from patients.

Echocardiography

Conventional 2D and Doppler echocardiography were performed using commercially available ultrasound equipment (iE33, Philips Medical Systems, Andover, MA, USA) with a S5-1 transducer by cardiologists who were expertly trained in echocardiography procedures. Comprehensive 2D and Doppler echocardiographic examinations was performed in all study patients. Biplane Simpson LV volumes and LVOT gradient were obtained by a simplified Bernoulli equation. LVOT obstruction was defined as a peak resting gradient ≥50 mm Hg on Doppler echocardiography. LV mass was calculated using the formula validated by Devereux et al.[24]

Acquisition of cardiac CT images

CT examination were performed using a second generation dual-source CT system (Somatom definition; Siemens Medical Solution, Forchheim, Germany). The scan was acquired after injection of 60-80 mL of iomeprol-400 (Iomeron, Bracco Imaging SpA, Milan, Italy), followed by 40 mL of a 30:70 mixture of contrast and saline. Retrospective electrocardiography scanning with pulsing (30-80%) was performed, and tube current modulation based on patient's body size was utilized in effort to reduce radiation dose. Mean estimated radiation effective dose was 8.4 mSv. The imaging parameters included: detector collimation 64 × 0.6

mm, gantry rotation time 280 ms, pitch 0.17-0.38 (adapted to the heart rate), tube current 240-450 mA, and tube voltage 80-120 kV.

Three-dimensional reconstruction of CT images

Using customized software (A-View Cardiac, Asan Medical Center, Korea), we could obtain cardiac CT images of 3 projection views; axial, sagittal, and coronal views. We could draw LV masks by using the difference of Hounsfield unit and correct LV masks manually according to LV myocardium on each cross-sectional image of the CT (**Figure 1**). We separated the PMs from the LV mask (**Figure 2**). Representative images of each group - ASH with LVOT obstruction, ASH only, apical HCMP, and normal – are shown in **Figure 3**.

Calculation of LV and PM mass and realignment of the LV

After completing the masks of the LV and PMs, we could automatically calculate the volume of the LV and the PMs. To get LV and PM mass value, we multiplied the value of the volume of the LV and the PMs by the average organ density (1.0527 g/ml).[25]

In terms of 3D coordinate, we realigned XYZ-coordinates of the LV by positioning LV apex to inferior and LV base to superior (**Figure 4**). The direction of anterior to posterior and medial to lateral was maintained to the original orientation (**Figure 5**). In detail, we placed the zero point of XYZ-coordinate of axial and coronal images in the center of LV cavity (**Figure 6**), and then turned the X-axis in the counterclockwise direction until we can see the exact LV apex in the coronal view (**Figure 7**). In the coronal view, we turned the X-axis until the Z axis is adjusted to and parallel to the LV axis (**Figure 8**). After rearranging the LV according to the modified axis, final images and axis of 3D coordinates could be shown as described above. (**Figure 4, 5**) The zero point of the 3D coordinate axis was repositioned to the center of the MV annulus

Calculation of the tip and the center of mass (barycenter) of a PM

The tip of a PM was defined as the highest point of each PM in z-coordinate.

A method to locate the 3D coordinates of the center of mass begins by supporting the

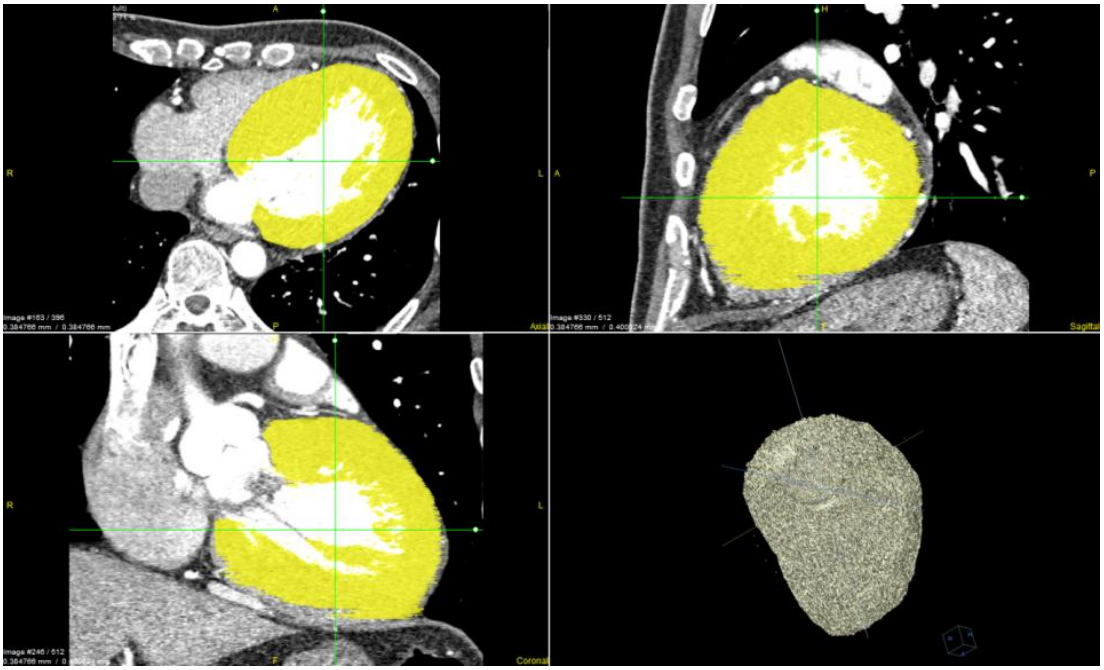

Fig 1. Three-dimensional reconstruction of the LV using cardiac CT.

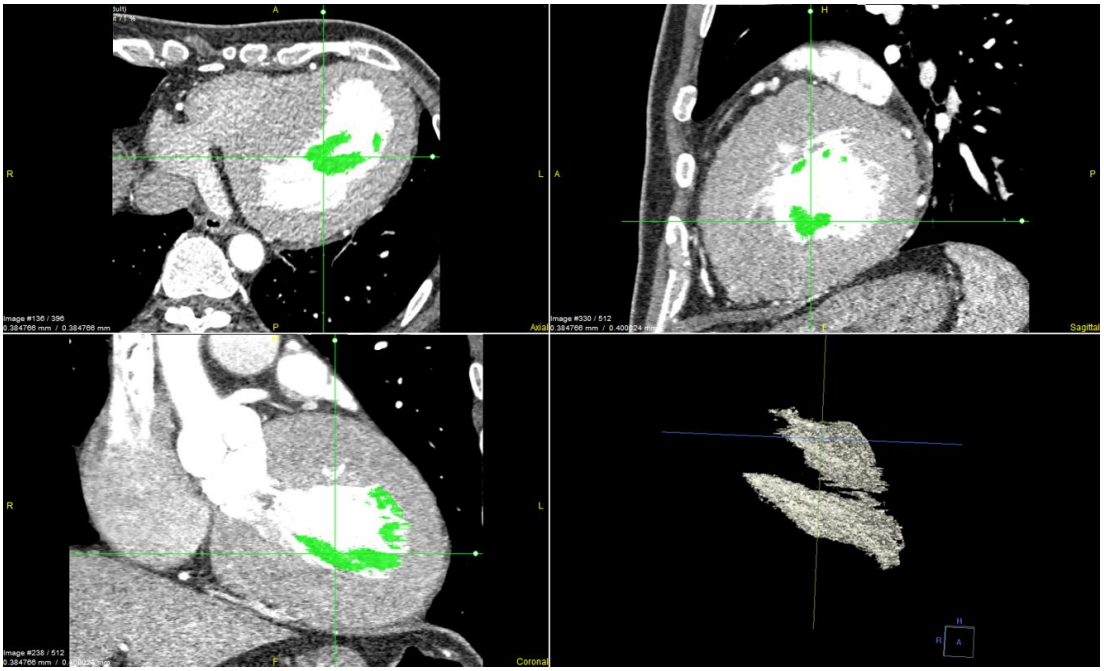

Fig 2. Three-dimensional reconstruction of the PM using cardiac CT.

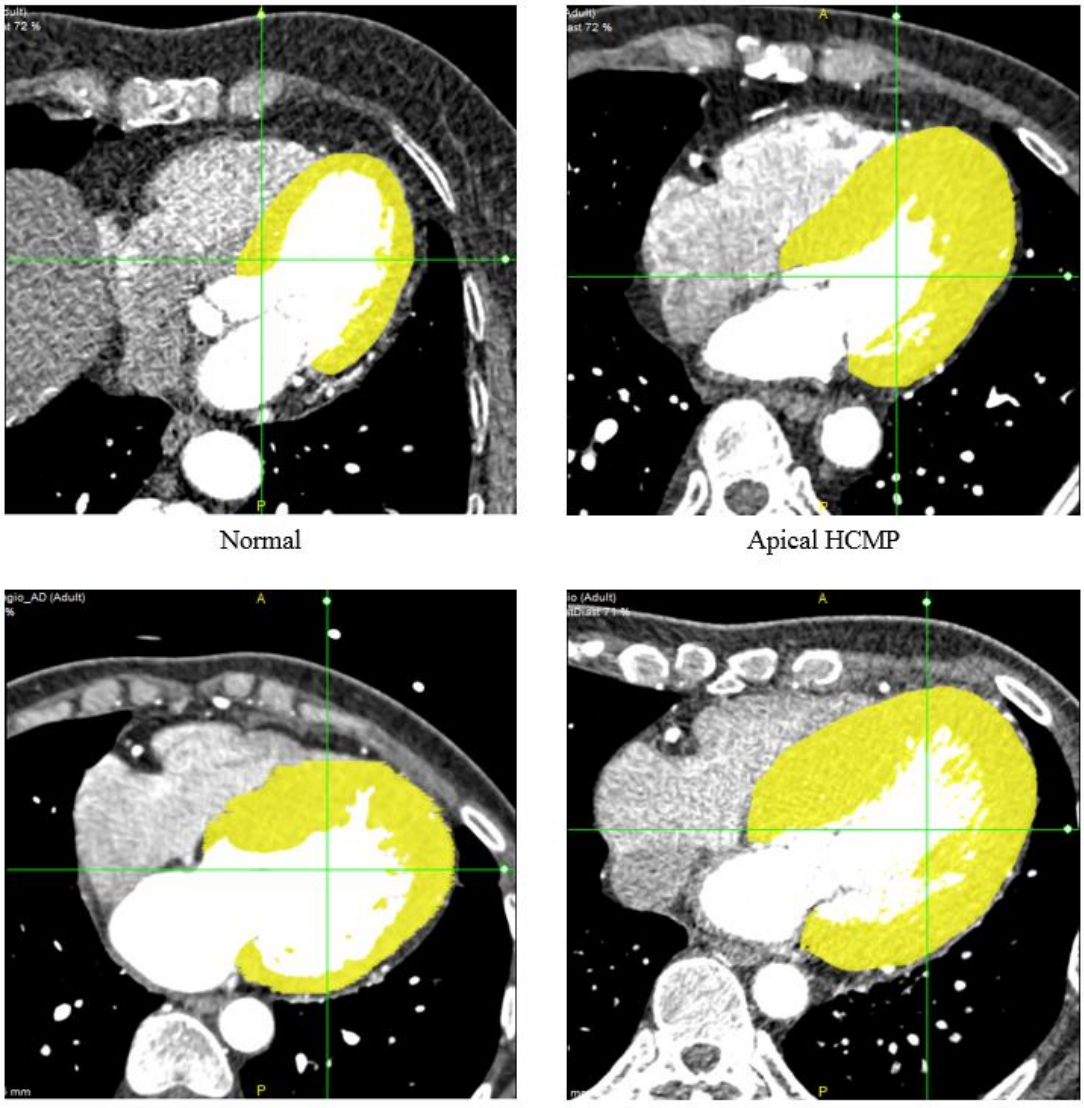

Fig 3. Representative images of each group.

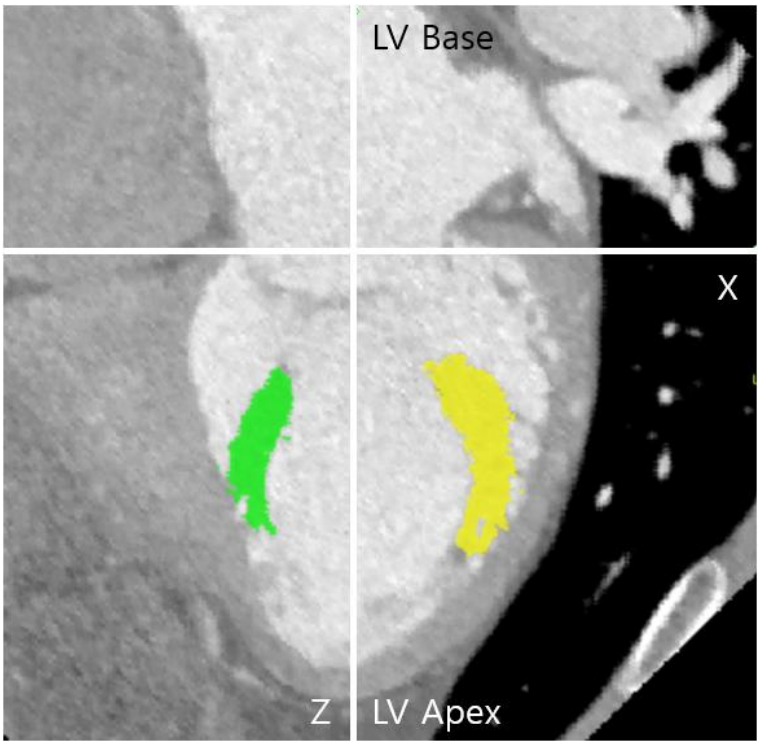

Fig 4. XZ-coordinate axis on long axis view of the LV.

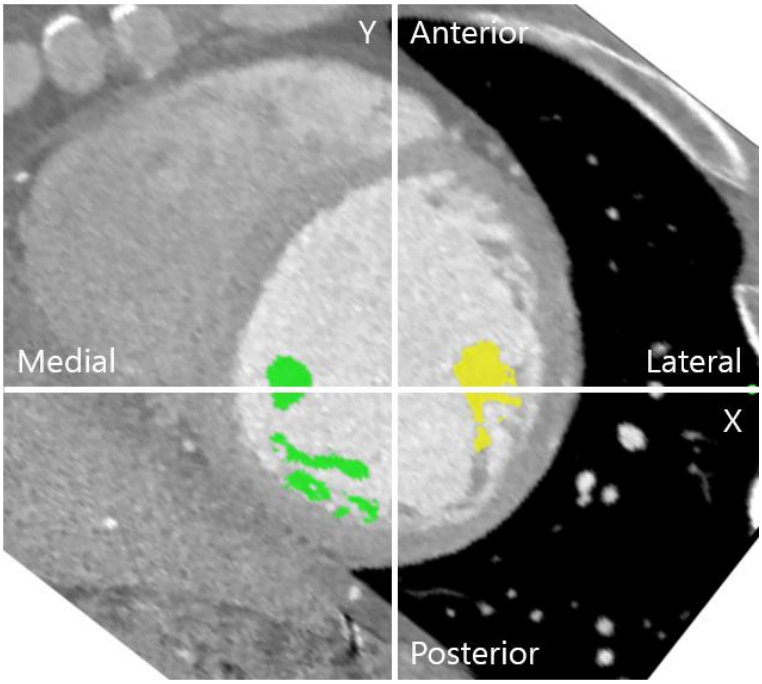

Fig 5. XY-coordinate axis on short axis view of the LV.

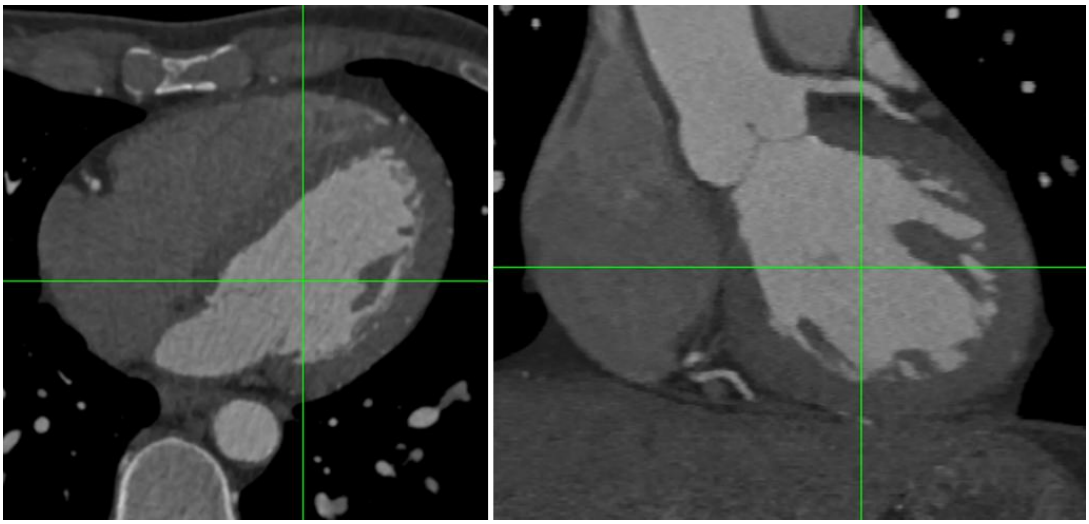

Axial view Coronal view

Fig 6. Placement of the zero point of XYZ coordinate in the center of LV cavity

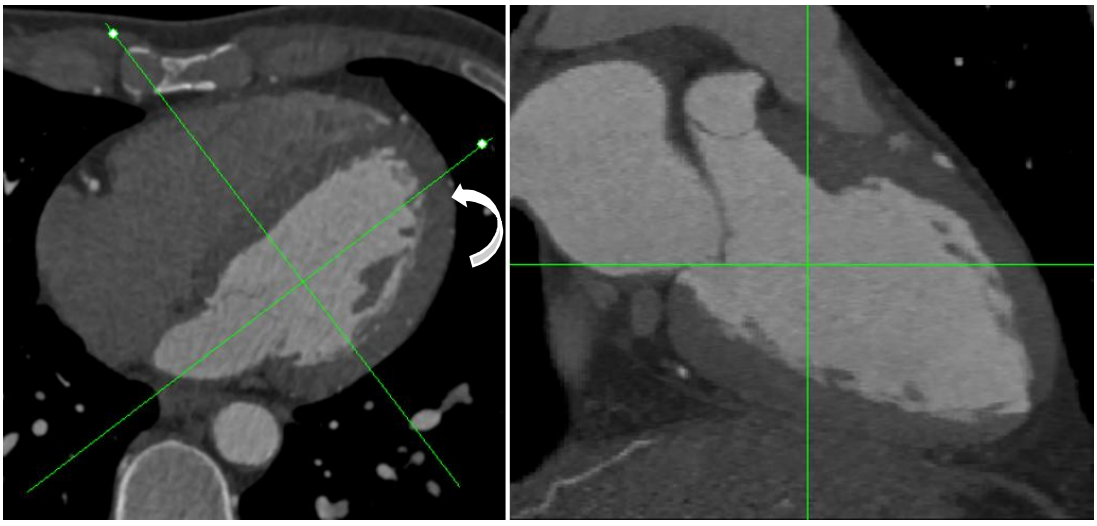

Axial view Coronal view

Fig 7. Turning the XY-axis in the counterclockwise direction until LV apex appears in the coronal view.

Coronal view

Fig. 8. Turning the XZ-axis in the counterclockwise direction until the Z axis is parallel to LV cavity and apex

object at three points and measuring the forces, F1, F2 and F3 that resist the weight of the PM, W = -$W\check{\mathrm{k}}$ ($\check{\mathrm{k}}$ is the unit vector in the vertical direction). Let r1, r2 and r3 be the position coordinates of the support point, then the coordinates R of the center of mass satisfy the condition that the resultant torque is zero,

$$\mathrm{T} = (\mathrm{r1} - \mathrm{R}) \times F1 + (r2 - R) \times F2 + (r3 - R) \times F3 = 0, \text{ or}$$

$$\mathrm{R} \times \left(-W\check{\mathrm{k}}\right) = r1 \times F1 + r2 \times F2 + r3 \times F3$$

This equation yields the coordinates of the center of mass R* in the horizontal plane as,

$$\mathrm{R}* = -\frac{1}{W}\check{\mathrm{k}} \times (\mathrm{r1} \times \mathrm{F1} + \mathrm{r2} \times \mathrm{F2} + \mathrm{r3} \times \mathrm{F3}).$$

The center of mass lies on the vertical line L, given by

$$\mathrm{L}(t) = R* + t\check{\mathrm{k}}$$

The 3D coordinates of the center of mass are determined by performing this experiment twice with the PM positioned so that these forces are measured for two different horizontal planes through the PM. The center of mass will be the intersection of the two lines L1 and L2 obtained from the two experiments.

We revised all coordinate values to millimeter unit by multiplying the slice thickness of CT images and pixel spacing.

Statistical Methods

Continuous variables are expressed as mean ± standard deviation. Categorical variables are expressed as frequency with percentage. Statistical significance between patient's characteristics with and without LVOT obstruction was determined using Student's *t*-test or Wilcoxon rank-sum test (if the assumption of normality is violated on Shapiro-Wilk normality test) for continuous measures, while the χ^2 test was used to compare categorical variables. Logistic regression analysis was employed to determine which factors were associated with LVOT obstruction in each subgroup. For the latter analysis, only covariates with a *P*-value

<0.05 were retained for further analysis. A *P* value <0.05 was considered to be statistically significant. Statistical calculation was computed using SPSS version 21.0

RESULTS

Baseline characteristics and echocardiographic findings

Demographic characteristics and echocardiographic findings of study population are shown in **Table 1**. Age, sex, body surface area, and LV ejection fraction were not significantly different among study groups. Mean age was 61±11 years old with 71.7% men. LV end-systolic and end-diastolic volume was significantly larger in normal group than those of HCM groups. LV mass, indexed to body surface area, was significantly higher in the order named; the group of ASH with LVOT obstruction, ASH only, apical HCM, and normal control.

The mass of the LV and the PM from 3D reconstruction of cardiac CT

Mass of the LV of each group, indexed to body surface area (BSA), was significantly increased in the order named-the group of normal control, apical HCM, ASH only, and ASH with LVOT obstruction-, which was similar with echocardiographic findings (**Table 2**). The mass of septum was not different between the groups of ASH with LVOT obstruction and ASH only. Furthermore, indexed anterolateral PM mass was increased sequentially comparable to indexed LV mass according to each group. Indexed anterolateral PM was significantly more massive than indexed posteromedial PM in each group (**Table 3**). The ratio of anterolateral PM mass to posteromedial PM mass and the difference of both PM mass seemed to increase sequentially. However, the ratio and difference of PM mass was similar between ASH only group and ASH with LVOT obstruction group.

Table 1. Demographic characteristics and echocardiographic findings of study population

	Normal (n=30)	**Apical HCM (n=30)**	**ASH only (n=30)**	**ASH+LVOT obstruction (n=30)**	***P* value**
Age	60±9	65±8	61±12	58±12	0.234
Male sex, %	70	76	76	63	0.614
Body surface area, m^2	1.77 [1.65;1.88]	1.82 [1.63;1.93]	1.75 [1.61;1.92]	1.69 [1.58;1.90]	0.662
LV end-systolic volume, cm^3	34.5 [30;40]	26 [23;35]	29 [22;33]	27.5 [21;34]	0.001
LV end-diastolic volume, cm^3	94.5 [76;109]	76 [60;89]	84 [61;93]	81 [63;95]	0.009
Interventricular septal thickness, mm	9.0 [8.0;10.0]	10.5 [10.0;13.0]	18.0 [17.0;20.0]	19.5 [17.0;20.0]	<0.001
LV ejection fraction, %	63.5±3.5	63.8±5.0	64.2±4.7	65.1±5.9	0.180
LV mass, g	155.2±39.6	196.2±38.3	267.4±72.1	280.2±82.7	<0.001
LV mass index, g/m^2	89.1 [80.0;96.6]	112.6 [94.4;126.0]	146.2 [123.4;184.9]	158.0 [125.3;193.2]	<0.001

Table 2. Data of 3D reconstruction of cardiac CT of study population

	Normal (n=30)	**Apical HCM (n=30)**	**ASH only (n=30)**	**ASH+LVOT obstruction (n=30)**	***P* value**
Indexed LV mass	74.6 [61.7;86.2]	111.2 [98.1;125.5]	124.2 [105.3;143.7]	143.1 [118.2;189.7]	<0.001
Indexed anterolateral PM mass	2.55 [1.71;2.92]	3.63 [2.44;5.07]	4.29 [2.94;5.01]	5.04 [3.40;7.11]	<0.001
Indexed posteromedial PM mass	2.04 [1.56;2.39]	2.43 [1.97;2.76]	1.83 [1.40;2.80]	3.38 [1.92;5.17]	0.009
Anterolateral PM to posteromedial PM mass ratio	1.19 [0.92;1.41]	1.57 [1.24;1.95]	1.78 [1.52;2.46]	1.72 [1.48;2.68]	<0.001
Difference of both PM mass indexed by LV mass	0.004±0.01	0.012±0.013	0.015±0.012	0.016±0.018	0.001
Indexed interventricular septum mass			31.33	35.95	0.075

Table 3. Comparison of each indexed PM mass according to each group

	Indexed Anterolateral PM Mass	**Indexed Posteromedial PM Mass**	***P* value**
Normal	2.55 [1.71;2.92]	2.04 [1.56;2.39]	<0.001
Apical HCMP	3.63 [2.44;5.07]	2.43 [1.97;2.76]	<0.001
ASH only	4.29 [2.94;5.01]	1.83 [1.40;2.80]	<0.001
ASH+LVOT obstruction	5.04 [3.40;7.11]	3.38 [1.92;5.17]	<0.001

Three-dimensional coordinates of the center of the aortic valve and the tip/barycenter of the PMs

We could obtain 3D coordinates of the center of the aortic valve (AV) and both PM tip/barycenter (**Table 4**). Median XY-coordinates (short axis view, **Figure 5**) of centroid of the AV and the tip/barycenter of both PMs are shown in **Figure 9 and 10**.

In the XY-plane (short axis view), the coordinate point of the tip of the anterolateral PM seemed to be similar among each group. However, the coordinate point of the barycenter of the anterolateral PM seemed to be displaced toward anterior and lateral direction in the order named previously. In terms of the posteromedial PM, the tip of the posteromedial PM seemed to be displaced toward lateral direction and the barycenter of the posteromedial PM also seemed to be displaced from medial to lateral and anterior direction sequentially.

The inter-tip distance of both PMs seemed to get shorter sequentially in the XY-plane (short axis view, **Table 2**, **Figure 5**). However, in the 3D coordinate, the inter-tip distance of both PMs was not different among each group due to changes of z-coordinate of the anterolateral PM tip (**Table 2, Figure 11**).

Z-coordinate of center of the aortic valve and tip/barycenter of both papillary muscles

We could observe the mass of both PMs in cardiac CT to increase as LV mass increases in each group. The Z coordinate of the tip of the anterolateral PM approaches to LV base as LV mass increases, contrary to the barycenter of the anterolateral PM, which was similar in the z-coordinate of each group. (**Figure 11**) This finding might imply that the anterolateral PM elongates as the mass of the anterolateral PM increases, however, the posteromedial PM gets thicker, rather than elongated, as LV mass increases.

Independent predictive factor of LVOT obstruction

In univariate analysis for LVOT obstruction, several factors were significantly associated with LVOT obstruction, such as LV mass index, anterolateral PM mass index, posteromedial PM mass index from cardiac CT, X and Y coordinates of barycenter of the anterolateral PM, X

Table 4. Three-dimensional coordinate of aortic centroid and PM tip/barycenter

	Normal (n=30)	**Apical HCM (n=30)**	**ASH only (n=30)**	**ASH+LVOT obstruction (n=30)**	***P* value**
Anterolateral PM tip					
X	18.8 [14.5;21.3]	17.9 [13.0;20.8]	19.4 [15.3;23.7]	19.8 [16.1;23.7]	0.470
Y	7.0 [-0.9;9.5]	7.5 [1.5;15.5]	5.4 [-4.1;13.4]	2.3 [-5.1;12.6]	0.400
Z	-24.2 ± 6.3	-22.3 ± 8.3	-20.2 ± 9.5	-15.8 ± 9.9	<0.001
Anterolateral PM barycenter					
X	20.5 ± 3.8	17.6 ± 5.0	21.6 ± 8.0	25.2 ± 5.4	<0.001
Y	3.2 ± 5.0	5.1 ± 5.7	6.3 ± 6.1	9.0 ± 7.6	<0.001
Z	-54.3 [-61.8;-43.8]	-59.7 [-63.6;-52.8]	-58.8 [-65.4;-53.4]	-59.4 [-64.8;-49.2]	0.247
Posteromedial PM tip					
X	-8.9 [-12.4;-2.0]	-7.0 [-12.0;-1.7]	-4.0 [-10.0;1.8]	-2.3 [-4.6;3.3]	0.003
Y	-3.3 [-12.0;3.8]	-9.3 [-12.6;-2.6]	-3.8 [-14.3;5.7]	-0.9 [-12.5;5.3]	0.432
Z	-33.6 [-38.4;-25.2]	-33.9 [-42.0;-24.0]	-33.6 [-39.6;-25.2]	-36.6 [-41.4;-24.0]	0.914
Posteromedial PM barycenter					
X	-3.3 ± 5.2	-0.8 ± 4.2	2.2 ± 4.9	7.2 ± 5.7	<0.001

Y	-5.0 ± 4.6	-3.3 ± 4.4	-4.0 ± 5.0	-1.3 ± 6.7	0.017
Z	-63.6 [-70.2;-52.2]	-68.4 [-72.0;-58.8]	-67.8 [-73.2;-60.6]	-69.3 [-79.2;-64.2]	0.041
Aortic valve center					
X	-0.6 [-6.5;3.4]	0.6 [-3.6;4.9]	1.2 [-2.2;4.0]	-0.2 [-2.9;2.0]	0.572
Y	27.6 [25.6;29.8]	27.5 [26.0;29.9]	27.8 [26.6;29.2]	27.8 [25.2;29.7]	0.980
Z	2.8 ± 5.5	3.5 ± 5.1	7.6 ± 6.3	11.5 ± 7.8	<0.001
Inter PM tip distance (3D), mm	30.6 [27.5;34.0]	30.5 [26.3;38.9]	30.0 [25.4;37.9]	29.0 [25.0;31.8]	0.269
Inter PM tip distance (xy plane), mm	30.3 [26.4;32.5]	29.4 [25.9;35.8]	27.8 [23.2;31.4]	26.0 [19.4;27.9]	0.005
Inter tip-barycenter distance (AL PM)	30.0±8.5	36.9±10.2	38.8±8.7	44.9±10.7	<0.001
Inter tip-barycenter distance (PM PM)	30.7 [27.1;34.5]	33.8 [28.1;39.5]	33.5 [27.8;40.1]	40.8 [34.7;50.0]	<0.001

The center of the MV annulus is the zero point.

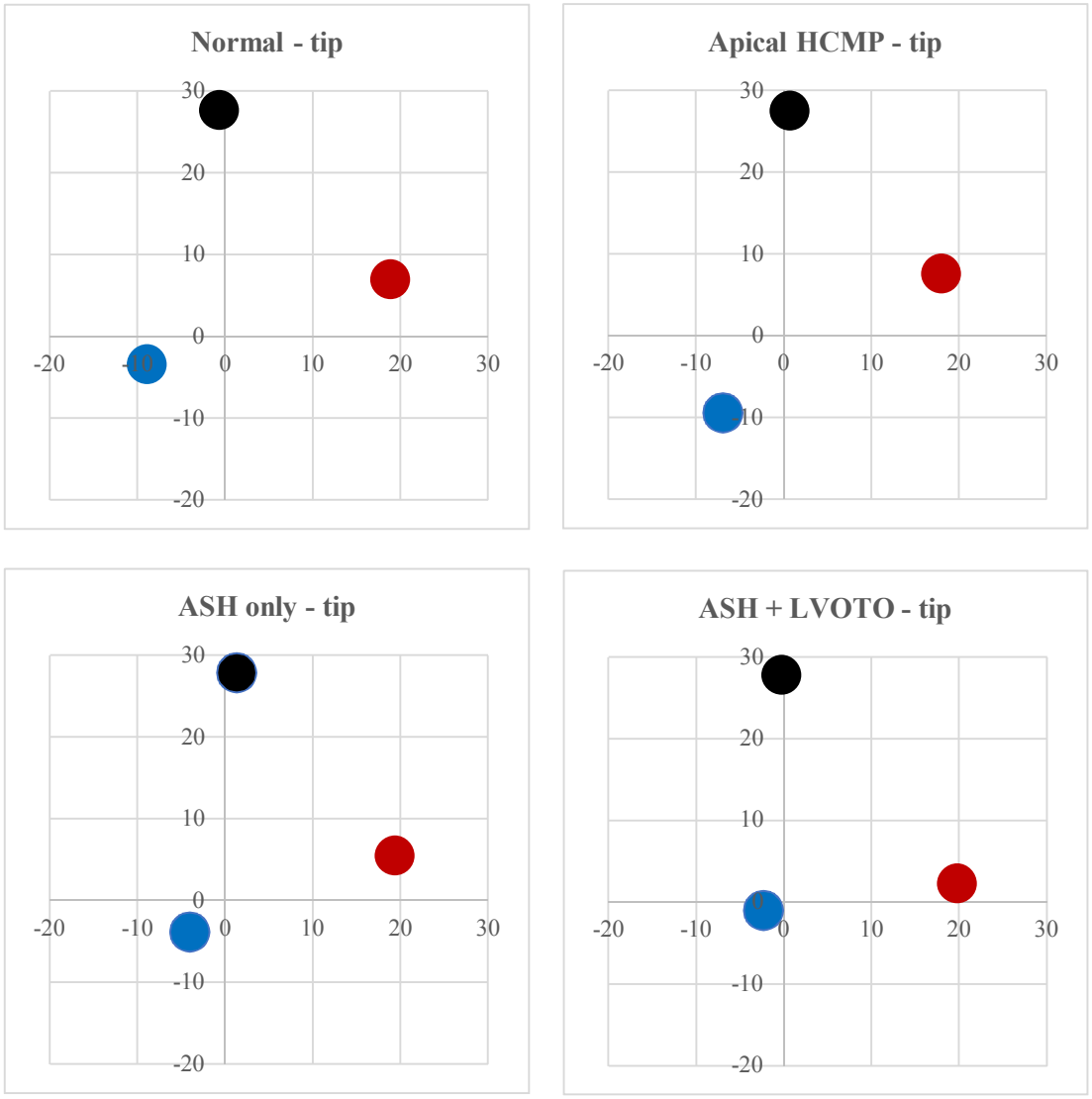

Fig 9. XY-coordinate of the center of the aortic valve and the tips of both PMs according to each group.

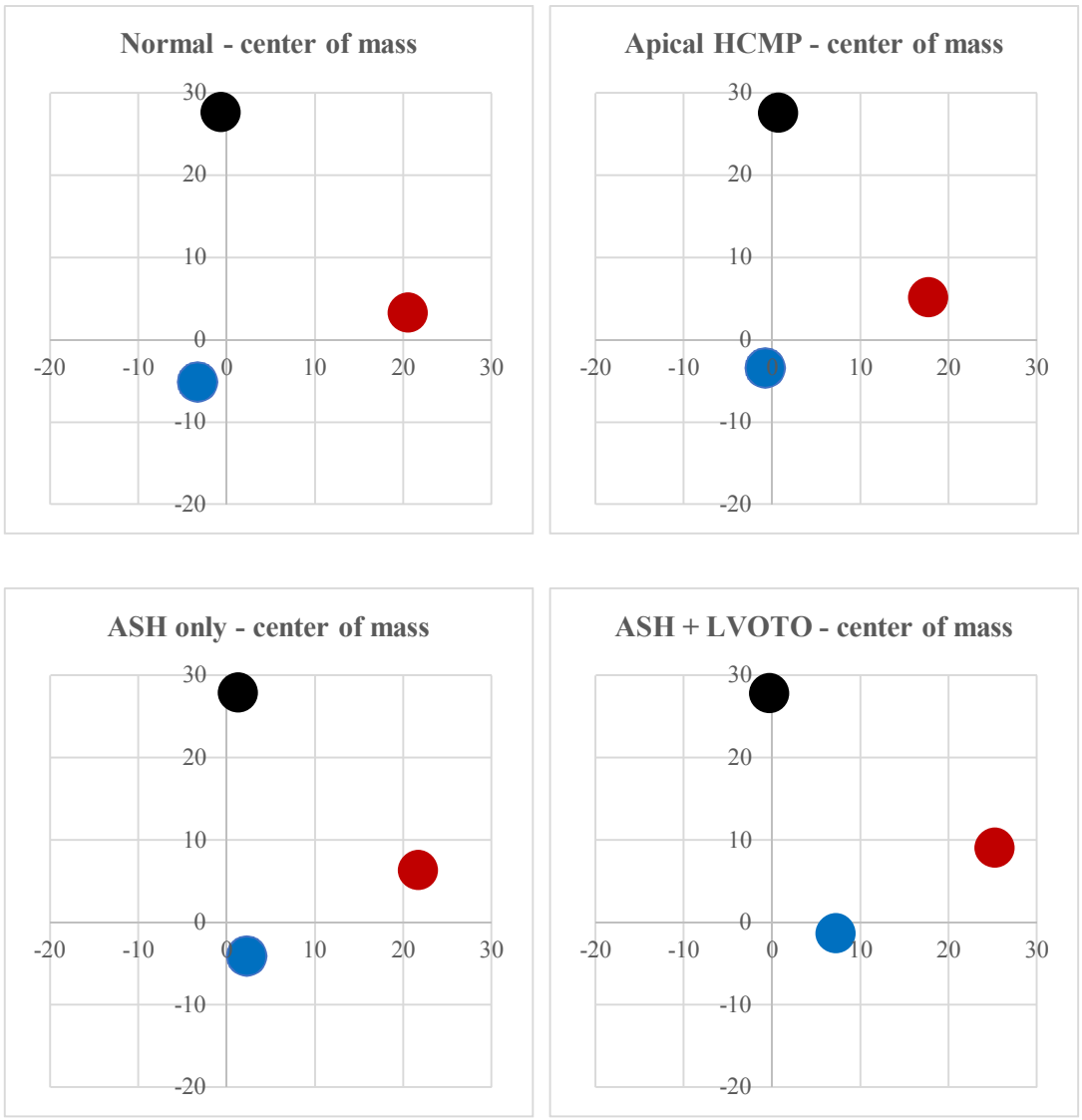

The center of MV annulus is the zero point.

Anterolateral PM Posteromedial PM Center of Aortic Valve

Fig 10. XY-coordinate of the center of the aortic valve and the center of mass of both PMs according to each group.

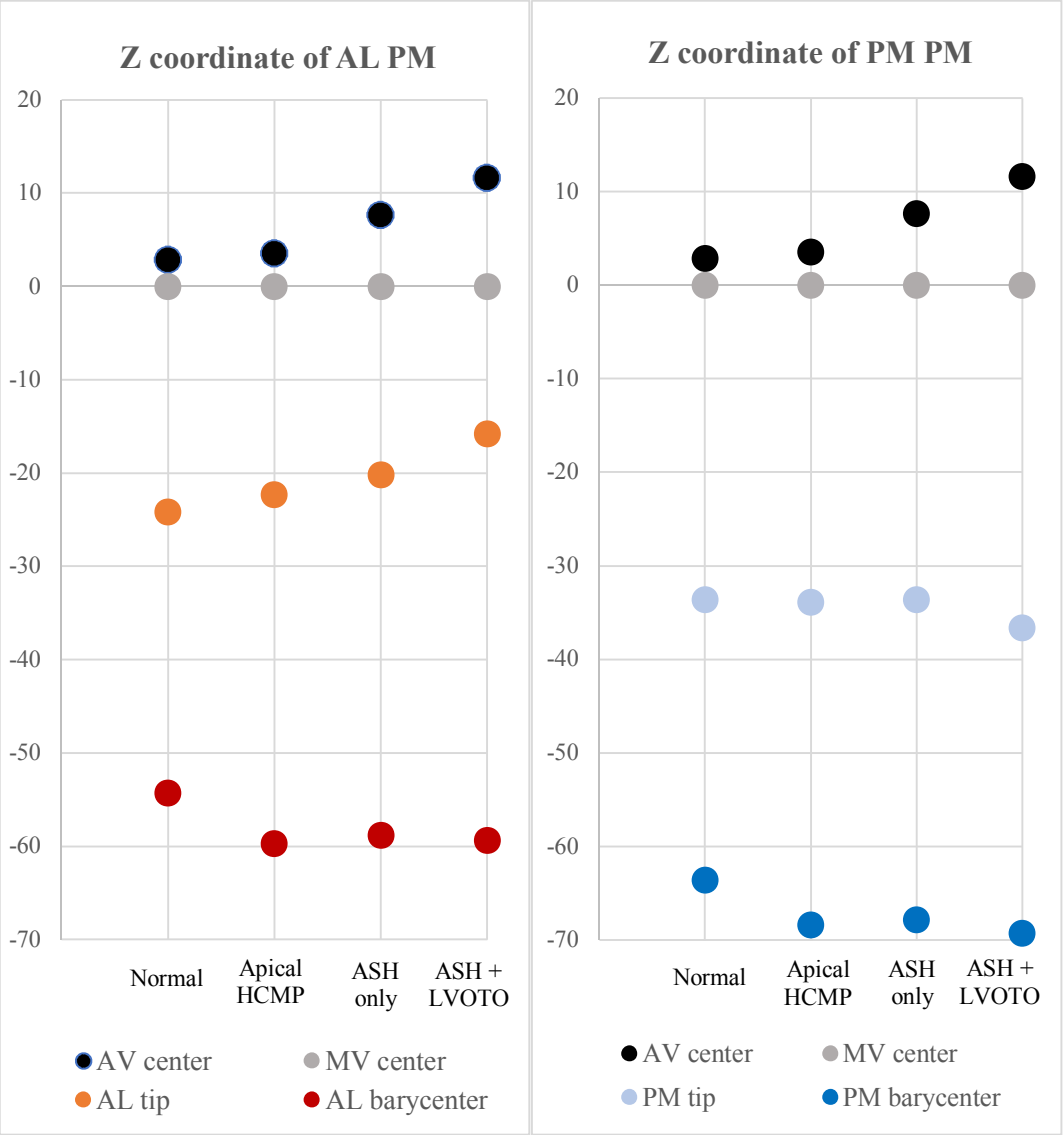

The center of the MV annulus is the zero point.

Fig 11. Z-coordinate of the center of the aortic valve and the center of mass/tip of both PMs according to each group.

coordinate of barycenter of the posteromedial PM, and X coordinate of tip of the posteromedial PM. After adjusting for retained covariates, displacement from medial to lateral direction of the barycenter of the posteromedial PM (adjusted odds ratio [OR] 0.808, 95% confidence interval [CI] 0.718-0.909, *P* value <0.001) was independently associated with LVOT obstruction (**Table 5**).

Correlation and linear regression analysis for lateral displacement of barycenter of the posteromedial PM

In unadjusted bivariate correlation analysis, several variables were significantly correlated to lateral displacement of the posteromedial PM, such as indexed LV mass, indexed posteromedial PM mass, septum mass, and interventricular septum thickness measured by echo. (**Table 6**) In multivariate linear regression analysis, indexed PM mass was an only independent contributing factor for lateral displacement of barycenter of the posteromedial PM. (**Table 7**)

Table 5. Multivariate logistic regression for LVOT obstruction

	Adjusted Odds Ratio	**95% CI**	***P* value**
Posteromedial PM barycenter X	0.866	0.765-0.980	<0.023

Table 6. Bivariate correlation analysis for lateral displacement of posteromedial PM

	Indexed LV mass (CT)	Indexed posteromedial PM mass (CT)	Indexed IVS mass (CT)	IVST (echo)
Posteromedial PM barycenter X	r=0.473 (*P* <0.001)	r=0.365 (*P* <0.001)	r=0.416 (*P*=0.001)	r=0.553 (*P* <0.001)

PM=papillary muscle, LV=left ventricle, IVS=interventricular septum, IVST=interventricular septum thickness

Table 7. Multivariate linear regression analysis for lateral displacement of posteromedial PM

	Beta coefficient	**95% CI**	**P value**
Indexed LV mass (CT)	-0.124	-0.071 ~ 0.039	0.557
Indexed posteromedial PM mass (CT)	0.448	0.543 ~ 2.593	0.003
Septum mass (CT)	0.239	-0.077 ~ 0.359	0.199
IVST (echo)	0.076	-0.299 ~ 0.521	0.591

PM=papillary muscle, LV=left ventricle, IVS=interventricular septum,

IVST=interventricular septum thickness, CI=confidence interval

DISCUSSION

Normal anatomy and mass of the PM

Two PMs attaches to the middle third of medial and lateral side of its posterior wall beneath the mitral valve commissures, with tips overhanging more basal left ventricular wall segment.[26] The anterolateral PM generally has a single head and the posteromedial PM often has two heads.[27,28] Meanwhile, accessory PMs can be found in approximately 15% of otherwise normal hearts.[13] Normal end-diastolic PM length is approximately 3.0 cm, with a fractional shortening of about 20%.[29] The combined mass of the PMs is normally ≤ 7 g/m^2 when measured using cardiac magnetic resonance imaging.[13] PM hypertrophy, defined as a combined mass >7 g/m2, occurs in more than half of patients with HCM.

In this study, we made a complete in-vivo 3D LV and PM evaluation from CT images and combined mass of both PMs were 9.24 g/m^2 for ASH with LVOT obstruction, 6.32 g/m^2 for ASH only, 6.31 g/m^2 for apical HCM, and 4.72 g/m^2 for normal control. Notably, anterolateral PM mass indexed to BSA was significantly larger than indexed posteromedial PM mass in all study groups. (**Table 3**) The ratio of indexed mass of the anterolateral PM to that of the posteromedial PM increased as LV mass increases. However, the ratio and difference of the anteraolateral PM and the posteromedial PM between the groups of ASH with LVOT obstruction and ASH only group was not significant. Therefore, mass difference of the PMs between the groups of ASH with LVOT obstruction and ASH only did not contribute to LVOT obstruction in this study.

Three-dimensional coordinates of the tip and the barycenter of the PM

As we mentioned earlier, we made 3D XYZ-coordinate axis by realigning the LV – LV apex to inferior and LV base to superior – and the center mark was positioned to the centroid of the MV annulus. (**Figure 4, 5**) In this 3D coordinates, we demonstrated the median values of the tips and the barycenters of the anterolateral and the posteromedial PM in the XY plane, similar to parasternal short axis view of the LV in 2D echocardiography. (**Figure 9, 10**) From the

complete 3D coordinates, we identified the displacement of the barycenter of the postermedial PM was the only independent predictive factor for LVOT obstruction.

In previous reports, the tips of the PMs in HCM patients face inward, toward one another (medial displacement), reducing inter-PM distance.[14,17] This geometric alteration is considered to promote LVOT obstruction because it produces slack in those chords attached to the center (A2 segment) of the anterior mitral leaflet, allowing it to be swept anteriorly (systolic anterior motion) toward the septum.

In the present study, inter-PM tip distance on XY plane (short axis view) seems to reduce as LV mass increases, however, inter-PM tip distance in the 3D XYZ axis of coordinates was not different among study groups. Although anterior and medial displacement of tip of both PM makes inter-PM distance get shorter on XY plane (2D), real 3D distance between the tips of both PM was similar due to the difference of Z coordinate of both PM tips. This difference creates distance between both PM tips in Z coordinates despite of reduced inter-PM distance on the XY plane, which makes the distance of inter-PM tip in the 3D coordinates similar among study groups.

Although both PMs seems to displace anteriorly and medially in the group of ASH with LVOT obstruction, the tip and barycenter of both PMs was not diaplaced evenly in this study. In the XY plane (short axis view), the tip of the posteromedial PM moved from medial to lateral direction, however, the tip of the anterolateral PM stayed at the almost same position. In terms of the barycenter of both PMs, the barycenter of the anterolateral PM seemed to move anteriorly, however, the barycenter of the posteromedial PM moved anteriorly and laterally.

Contributing factors for lateral displacement of barycenter of the posteromedial PM

As we mentioned above, lateral displacement of the barycenter of the postermedial PM was the only independent predictive factor for LVOT obstruction. Therefore, we investigated the contributing factors for lateral displacement of barycenter of the posteromedial PM. The degree of lateral displacement was well correlated with indexed LV mass, indexed

posteromedial PM mass, septum mass, and thickness of interventricular septum measured by 2D echo. (**Table 6**). In multivariate analysis, only indexed PM mass was independently associated with lateral displacement of barycenter of the posteromedial PM. As LV mass increases, both PM mass also increases. In **Figure 11**, tip of the anterolateral PM approaches to LV base, which might imply that anterolateral PM gets elongated. On the contrary, tip of the posteromedial PM remains the same position as LV mass increases, which might imply that the posteromedial PM gets thicker. By extension, we can assume that this different pattern of hypertrophy of the PM can affect lateral displacement of barycenter of the posteromedial PM.

We also presumed that thickness or increased mass of septum might be important because increased thickness or mass of septum could extrude the base of medial PM to lateral direction. Although the interventricular septum measured by 2D echo was significantly thicker in the ASH groups than in the group of apical HCM and normal control, the thickness of interventricular septum between the groups of ASH with LVOT obstruction and ASH only was not different statistically. (**Table 2**). Futhermore, although indexed LV mass and indexed septum mass was well correlated with the degree of lateral displacement of the posteromedial PM, indexed LV or septum mass were eliminated in the multivariate analysis. This finding might support the previous report that pattern of hypertrophy is important in terms of LVOT obstruction. As mentioned above, Song et al. reported spiral pattern of LV hypertrphy was more frequent in patients with ASH and LVOT obstruction.[23] We did not analyze the pattern of LV hypertrphy in the present study, however, the pattern of hypertrophy might be more important than the degree of LV hypertrophy in the pathophysiology of LVOT obstruction in patients with HCM.

Limitations

There are several limitations to be addressed. First, this is a retrospective, cross-sectional study which can potentially have selection bias and limit the interference of causal relationship of

LVOT obstruction. Second, the study population was relatively small in view of heterogenous characteristics of HCM patients. Lastly, we reconstructed the LV and the PMs only, not mitral leaflets which is known to contribute to LVOT obstruction. Although displacement of the PMs should interpose the mitral leaflets into the LVOT, which pushes the leaflets toward the septum, we could not assess the interactions between displaced PMs and mitral leaflets contributing to systolic anterior motion and LVOT obstruction. However, to the best of our knowledge, this is the first complete in-vivo 3D evaluation of the LV and both PMs and we made the most objective assessment of the LV and the PMs, excluding the possibility of operators' preconception.

CONCLUSION

From complete 3D masks of the LV and the PMs from cardiac CT images, we could identify that mass of both PMs increases and the ratio of mass of the anterolateral PM to that of the posteromedial PM also increases as the LV mass increases. The hypertrophy pattern of both PMs was not same, while the anterolateral PM seems to get elongated, the posteromedial PM seems to get thicker in ASH with LVOT obstruction group compared to normal control. This difference resulted in the similar inter-PM tip distance in the 3D coordinates. The tips and the center of mass of both PMs in the groups of ASH with LVOT obstruction was not displaced evenly. Displacement of the tip and the barycenter of the posteromedial PM was notable. The independent predictors of the LVOT obstruction was from medial to lateral displacement of barycenter of the posteromedial PM, which might result from hypertrophic pattern of the posteromedial PM.

REFERENCES

1. Wigle ED, Rakowski H, Kimball BP, Williams WG. Hypertrophic cardiomyopathy. Clinical spectrum and treatment. Circulation 1995;92:1680-92.

2. Maron BJ, Maron MS, Semsarian C. Genetics of hypertrophic cardiomyopathy after 20 years: clinical perspectives. Journal of the American College of Cardiology 2012;60:705-15.

3. Klues HG, Schiffers A, Maron BJ. Phenotypic spectrum and patterns of left ventricular hypertrophy in hypertrophic cardiomyopathy: morphologic observations and significance as assessed by two-dimensional echocardiography in 600 patients. Journal of the American College of Cardiology 1995;26:1699-708.

4. Gersh BJ, Maron BJ, Bonow RO, et al. 2011 ACCF/AHA Guideline for the Diagnosis and Treatment of Hypertrophic Cardiomyopathy: a report of the American College of Cardiology Foundation/American Heart Association Task Force on Practice Guidelines. Developed in collaboration with the American Association for Thoracic Surgery, American Society of Echocardiography, American Society of Nuclear Cardiology, Heart Failure Society of America, Heart Rhythm Society, Society for Cardiovascular Angiography and Interventions, and Society of Thoracic Surgeons. Journal of the American College of Cardiology 2011;58:e212-60.

5. Maron BJ, Maron MS. Hypertrophic cardiomyopathy. Lancet 2013;381:242-55.

6. Pollick C, Rakowski H, Wigle ED. Muscular subaortic stenosis: the quantitative relationship between systolic anterior motion and the pressure gradient. Circulation 1984;69:43-9.

7. Maron BJ, Gottdiener JS, Perry LW. Specificity of systolic anterior motion of anterior mitral leaflet for hypertrophic cardiomyopathy. Prevalence in large population of patients with other cardiac diseases. Br Heart J 1981;45:206-12.

8. Spirito P, Maron BJ. Significance of left ventricular outflow tract cross-sectional area in hypertrophic cardiomyopathy: a two-dimensional echocardiographic assessment. Circulation 1983;67:1100-8.

9. Sasson Z, Yock PG, Hatle LK, Alderman EL, Popp RL. Doppler echocardiographic determination of the pressure gradient in hypertrophic cardiomyopathy. Journal of the American College of Cardiology 1988;11:752-6.

10. Klues HG, Maron BJ, Dollar AL, Roberts WC. Diversity of structural mitral valve alterations in hypertrophic cardiomyopathy. Circulation 1992;85:1651-60.

11. Moro E, ten Cate FJ, Leonard JJ, Hugenholtz PG, Roelandt J. Genesis of systolic anterior motion of the mitral valve in hypertrophic cardiomyopathy: an anatomical or dynamic event? European heart journal 1987;8:1312-21.

12. Mikami T, Hashimoto M, Kudo T, Sugawara T, Sakamoto S, Yasuda H. Mitral valve and its ring in hypertrophic cardiomyopathy--a mechanism creating surplus mitral leaflet involved in systolic anterior motion. Jpn Circ J 1988;52:597-603.

13. Harrigan CJ, Appelbaum E, Maron BJ, et al. Significance of papillary muscle abnormalities identified by cardiovascular magnetic resonance in hypertrophic cardiomyopathy. The American journal of cardiology 2008;101:668-73.

14. Hwang HJ, Choi EY, Kwan J, et al. Dynamic change of mitral apparatus as potential cause of left ventricular outflow tract obstruction in hypertrophic cardiomyopathy. Eur J Echocardiogr 2011;12:19-25.

15. Halpern DG, Swistel DG, Po JR, et al. Echocardiography before and after resect-plicate-release surgical myectomy for obstructive hypertrophic cardiomyopathy. J Am Soc Echocardiogr 2015;28:1318-28.

16. Minakata K, Dearani JA, Nishimura RA, Maron BJ, Danielson GK. Extended septal myectomy for hypertrophic obstructive cardiomyopathy with anomalous mitral papillary muscles or chordae. J Thorac Cardiovasc Surg 2004;127:481-9.

17. Kim DH, Handschumacher MD, Levine RA, et al. In vivo measurement of mitral leaflet surface area and subvalvular geometry in patients with asymmetrical septal hypertrophy: insights into the mechanism of outflow tract obstruction. Circulation 2010;122:1298-307.

18. Schoendube FA, Klues HG, Reith S, Flachskampf FA, Hanrath P, Messmer BJ. Long-term clinical and echocardiographic follow-up after surgical correction of hypertrophic

obstructive cardiomyopathy with extended myectomy and reconstruction of the subvalvular mitral apparatus. Circulation 1995;92:Ii122-7.

19. Kwon DH, Setser RM, Thamilarasan M, et al. Abnormal papillary muscle morphology is independently associated with increased left ventricular outflow tract obstruction in hypertrophic cardiomyopathy. Heart 2008;94:1295-301.

20. Kwon DH, Smedira NG, Thamilarasan M, Lytle BW, Lever H, Desai MY. Characteristics and surgical outcomes of symptomatic patients with hypertrophic cardiomyopathy with abnormal papillary muscle morphology undergoing papillary muscle reorientation. J Thorac Cardiovasc Surg 2010;140:317-24.

21. Greupner J, Zimmermann E, Grohmann A, et al. Head-to-head comparison of left ventricular function assessment with 64-row computed tomography, biplane left cineventriculography, and both 2- and 3-dimensional transthoracic echocardiography: comparison with magnetic resonance imaging as the reference standard. Journal of the American College of Cardiology 2012;59:1897-907.

22. Koo HJ, Yang DH, Oh SY, et al. Demonstration of mitral valve prolapse with CT for planning of mitral valve repair. Radiographics : a review publication of the Radiological Society of North America, Inc 2014;34:1537-52.

23. Song Y, Yang DH, B OH, et al. Geometric predictors of left ventricular outflow tract obstruction in patients with hypertrophic cardiomyopathy: a 3D computed tomography analysis. European heart journal cardiovascular Imaging 2017.

24. Devereux RB, Alonso DR, Lutas EM, et al. Echocardiographic assessment of left ventricular hypertrophy: comparison to necropsy findings. The American journal of cardiology 1986;57:450-8.

25. Vinnakota KC, Bassingthwaighte JB. Myocardial density and composition: a basis for calculating intracellular metabolite concentrations. Am J Physiol Heart Circ Physiol 2004;286:H1742-9.

26. Victor S, Nayak VM. Variations in the papillary muscles of the normal mitral valve and their surgical relevance. J Card Surg 1995;10:597-607.

27. Uemura T, Otsuji Y, Nakashiki K, et al. Papillary muscle dysfunction attenuates ischemic mitral regurgitation in patients with localized basal inferior left ventricular

remodeling: insights from tissue Doppler strain imaging. Journal of the American College of Cardiology 2005;46:113-9.

28. Madu EC, D'Cruz IA. The vital role of papillary muscles in mitral and ventricular function: echocardiographic insights. Clin Cardiol 1997;20:93-8.

29. Tischler MD, Rothfeld J. Papillary muscle fractional shortening is a determinant of heart shape in patients with prior myocardial infarction. The American journal of cardiology 1997;80:204-6.

국문요약

배경: 비후성 심근비대증 환자의 병태학적 주요 특징은 승모판막 기구의 형태학적 및 기능적 이상으로 말미암은 좌심실 유출로의 폐색이다. 하지만 비후성 심근비대증 환자에서의 좌심실 유출로 폐색의 기전은 아직 완전히 밝혀지지 않았다. 본 연구에서는 심장 컴퓨터 단층촬영 영상을 3 차원으로 재구성하여 생체 내 좌심실 및 유두근의 질량과 유두근의 위치 변화가 좌심실 유출로 폐색에 어떤 영향을 미치는지 분석하고자 한다.

방법 및 결과: 심장 컴퓨터 단층 촬영 및 심장 초음파를 시행한 120 명의 연구 대상자-좌심실 유출로 폐쇄가 동반된 비대칭중격비대 환자 30 명, 좌심실 유출로 폐쇄가 없는 비대칭중격비대 환자 30 명, 심첨부 비후성심근비대증 환자 30 명, 그리고 정상 대조군 30 명-를 후향적으로 모집하였다. 이 대상자들에게 시행한 심장 컴퓨터 단층 영상에서 맞춤형 소프트웨어를 이용하여 3 차원 좌심실 모형을 구축하였고, 이를 통해 좌심실과 유두근의 질량을 계산하였다. 3 차원으로 재구성한 영상을 좌심실 첨부가 아래쪽으로 좌심실 바닥이 위쪽으로 오도록 좌심실을 이동시켜 3 차원 좌표축을 재배열하였고 각 연구 집단에서 유두근의 끝부분과 무게중심점의 3 차원 좌표점을 계산하고 위치 변화를 분석하였다. 체표면에 따라 조정된 유두근의 질량은 정상 대조군, 심첨부 비후성심근비대증 환자군, 비대칭중격비대 환자군, 좌심실 유출로 폐쇄가 동반된 비대칭중격비대중 환자군 순으로 의미 있게 증가하였다. 앞가쪽 유두근 질량과 뒤안쪽 유두근 질량의 비와 차이는 좌심실 질량이 증가할수록 순차적으로 증가하였다. 좌심실 유출로 폐쇄의 독립적인 예측 인자는 뒤안쪽 유두근의 무게중심점이 외측으로 이동하는 것이었다. (조정 대응비 0.808; 95% 신뢰구간 0.718-0.909, P 값 <0.001)

결론: 심장 컴퓨터 단층 촬영 영상을 이용하여 좌심실과 유두근의 3 차원 모델을 구축함으로 비후성 심근비대증 환자에서 심근 질량이 증가할수록 두 유두근의

질량과 앞가쪽 유두근/뒤안쪽 유두근의 질량 비가 증가함을 확인할 수 있었다. 좌심실 유출로 폐쇄의 독립적인 예측 인자는 뒤안쪽 유두근 무게중심점이 외측으로 이동하는 것이었다.